Rotor Dynamics Analysis in Turbine Generator Applications

Author: Manu Bodagala

Date: 6/13/2024

Abstract

Rotor dynamics is a pivotal field in mechanical engineering that involves the analysis of lateral and torsional vibrations within rotating shaft systems, particularly within potentially high-stakes environments like turbine generators. Leveraging dynamic simulations and detailed rotor bearing analysis, this report explains how flexible rotor geometries, coupled with high rotational speeds, influence vibration characteristics. The modeling of rotor dynamics may allow for the implementation of Active Magnetic Bearings to enhance the predictability and control of such vibrations, aiming to sustain operational stability above critical speed thresholds. These systems require accurate modeling because they rely on dependable model-based rotor levitation controllers for optimal operation.

Techniques relating to the development framework for finite element models aimed at streamlining rotor dynamics analysis are presented in this report. An open-source software suite based on rotor dynamics principles was reviewed, including examples that demonstrate its application in real-world scenarios. This software package will be used as a basis to explore the development and verification of more specialized rotor dynamics analysis tools. Simplified models can be tested as proof of concept to show the initial viability and potential applications of this modeling approach in complex rotor-dynamic systems in high-performance environments such as propulsion units and turbine generator applications.

Contents

List of Figures

Nomenclature

α	Stiffness Parameter
δ	Stiffness Parameter
γ	Coupling Parameter
ν	Poisson's Ratio
ω	Angular Velocity
ω_d	Damped Natural Frequency
ω_n	Natural Frequency
Φ	Phase Angle
ρ	Density
θ	Rotation Angle
ξ	Damping Ratio
A	Cross-sectional Area
C	Damping Matrix
c	Damping Coefficient
d	Diameter
E	Elastic Modulus
F	Force
G	Gyroscopic Matrix
G	Shear Modulus
I	Moment of Inertia
J_p	Polar Moment of Inertia
J_t	Transverse Moment of Inertia
K	Stiffness Matrix
k	Stiffness
L	Length
M	Mass Matrix
m	Mass
N	Number of Elements

P	Inertia Ratio
Q	Generalized Displacement Vector for the Entire System
q	Generalized Displacement Vector
R	Radius
T	Torque

1 Introduction

1.1 Dynamic Rotorbearing Analysis

Rotor dynamics is a critical field in mechanical engineering that focuses on the behavior of rotating shafts and the forces that influence their motion. This area of study is crucial for ensuring the stability and efficiency of high-performance machinery used in various industrial applications, including energy production, automotive, aerospace, and particularly Turbine Generator (TG) systems. Turbine generators often demand exceptionally reliable and robust systems due to the severe consequences of any potential failures and the extreme operational environments involved.

TG systems, characterized by their need for high power output and reliability, operate under stringent conditions where any failure can lead to catastrophic outcomes. These systems often run at high speeds that surpass the first critical speed or resonance mode, which historically has been a challenging aspect of rotor dynamics. Ensuring a safe operational margin above these critical speeds while undergoing continuous operation near them is vital for maintaining the structural integrity and missionworthiness of the propulsion units in TG systems.

With regard to Active Magnetic Bearing (AMB) and control system implementation, if the rotor dynamics across all operating RPMs are known through modeling techniques, an efficient feedforward control loop could be implemented to compensate for lateral vibration and whirl phenomena preemptively. Adding a layer of robust or adaptive control could further enhance reliability, ensuring the system remains stable and performs well even when external disturbances occur or when there are slight mismatches between the model and actual system behavior. The modeling of rotor dynamics properties opens up the opportunity to use efficient control methodologies to manage rotor systems.

This report explores the development of rotor dynamics analysis software that implements a finite element analysis framework to be used for enhancing the understanding and predictive capabilities of rotor dynamics models. Additionally, it seeks to provide information on the finite element method's utility in designing better, more efficient AMBs and other critical components.

2 Theory

2.1 Overview

This section of the report elaborates on the theoretical underpinnings necessary for developing comprehensive models of rotor dynamic systems. The focus is on deriving equations of motion that capture the essential dynamics of rotating machinery, employing both modern analytical techniques and traditional approaches. To achieve this, we explore various modeling frameworks that enable a nuanced understanding of rotor behavior under operational stresses.

To begin, a detailed examination of continuous models that describe the rotor dynamics through partial differential equations. These models are crucial for understanding the spatial variations and time-dependent behavior of rotors under various loading conditions. Following this, we transition to lumped parameter models which simplify the rotor system into discrete masses, springs, and dampers aligned in the lateral, axial, and torsional directions. This approach transforms the continuous dynamics into manageable matrix equations, facilitating easier analysis and solution.

Subsequently, these lumped parameter models serve as the basis for constructing finite element models of the rotor system. By discretizing the rotor into finite elements, we can capture the detailed local dynamics and interactions within the system, which are often obscured in more simplified models. This step involves carefully integrating contributions from each component, ensuring that the model accurately reflects the physical characteristics of the rotor.

2.2 Föppl/Jeffcott Single Mass Rotor Model

In a single-mass Jeffcott rotor with rigid bearings, the rotor with mass m is located at the axial center of the shaft. The mass of the shaft in a Jeffcott rotor model is assumed to be negligible compared to the mass of the disk; therefore, it is modeled as mass-less in analysis. The geometric center of the disk C is located at the point (U_{xC}, U_{yC}) along the coordinate axis defined about the bearing center line, and the disk center of mass G is located at (U_{xG}, U_{yG}). The unbalance eccentricity e_u is the vector that connects points C and G, and represents the unbalance in the rotor disk. e_u is assumed to be parallel with the x-axis at the initial time t = 0. Finally, u_C is the displacement vector with phase angle Θ that connects the origin and the point C, and Φ is the angle between e_u and u_C [1].

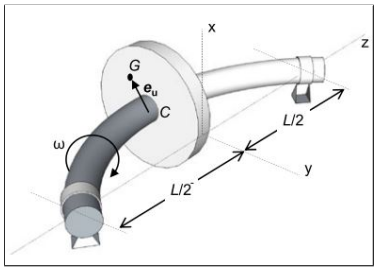

Figure 1: Single Mass Jeffcott Rotor [1]

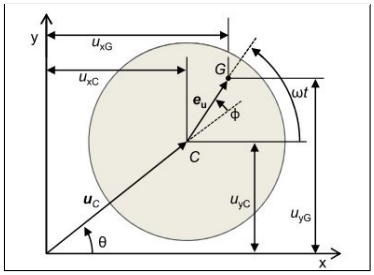

Figure 2: Back View of Mass [1]

Assuming that the rotor disk does not affect the stiffness of the massless shaft, the lateral

bending stiffness at the axial center of a simply supported uniform beam is given by,

$$k_s = \frac{48EI}{L^3} \tag{1}$$

where E is the elastic modulus of the beam, L is the length between the bearing and I is the shaft area moment of inertia [1]. For a uniform cylindrical shaft with diameter D, the equation for the area moment of inertia is [1],

$$I = \frac{\pi D^4}{64} \tag{2}$$

An assumption is made that there is a relatively small effective damping acting on the lateral motion of the disk at the rotor midspan, and the corresponding damping constant is given by c_s. This viscous damping combines shaft structural damping, fluid damping due to the flow in turbomachines, and the effective damping added by the bearings [1].

The dynamic model of the Föppl/Jeffcott rotor is derived using Newton's principles, targeting the rotor disk and assuming the shaft's mass to be negligible. This model incorporates the forces due to stiffness and damping as a consequence of shaft's lateral deformation. The equations describing the motion in the lateral directions, corresponding to the x and y axes as shown in Figure 1, are expressed in terms of the coordinates of the mass center and the geometric center. These coordinates are indicated by the subscripts G for the mass center and C for the geometric center. At any time t, the disk's mass center coordinates can be recalculated based on the geometric center and the rotation angle ωt of the rotor [2].

Integrating the second temporal derivatives of the coordinates of the mass center into the original lateral motion equations yields new expressions that describe the rotor's motion relative to the geometric center [1].

$$m\ddot{u}_{xG} = -k_s u_{xC} - c_s \dot{u}_{xC}, \tag{3}$$

$$m\ddot{u}_{yG} = -k_s u_{yC} - c_s \dot{u}_{yC}, \tag{4}$$

where (u_{xG}, u_{yG}) and (u_{xC}, u_{yC}) represent the coordinates of the mass center and the geometric center, respectively. The disk center of mass coordinates can be rewritten in terms of its geometric center C and the rotor angle of rotation ωt at time t,

$$u_{xG} = u_{xC} + e_u \cos(\omega t), \tag{5}$$

$$u_{yG} = u_{yC} + e_u \sin(\omega t). \tag{6}$$

By substituting the second derivatives from Eqs.s (5) and (6) into (3) and (4), we arrive at the equations of motion for the Föppl/Jeffcott rotor in terms of the disk geometric center:

$$m\ddot{u}_{xC} + k_s u_{xC} + c_s \dot{u}_{xC} = m e_u \omega^2 \cos(\omega t), \tag{7}$$

$$m\ddot{u}_{yC} + k_s u_{yC} + c_s \dot{u}_{yC} = m e_u \omega^2 \sin(\omega t). \tag{8}$$

The rigidity of the bearings is assumed to be perfect in this model, precluding any tilt of the rotor disk and thereby ignoring any gyroscopic effects on the rotor. With the shaft firmly anchored at the bearings, it maintains consistent alignment with the bearing centerline. This aspect, along with the effects of aerodynamics and fluid-film coupling forces—emanating from the rotor's seals and impellers and due to be discussed in subsequent sections—are not taken into account in this simplified analysis. The resultant equations of motion, outlined in Eqs (7) and (8), demonstrate decoupled behavior in the x and y axes [1].

2.2.1 Undamped Free Vibration

In the context of undamped free vibration, we contemplate a rotor scenario where imbalance eccentricity and damping are considered negligible. This assumption streamlines the equations governing the rotor's motion in the x and y planes, eschewing the terms for damping and eccentricity.

For this single mass rotor model, the homogeneous second-order system solutions are represented as exponential functions of time. These solutions hinge on constants A_x and A_y, which are contingent on the rotor disk's initial conditions. Reintroducing these solutions into the motion's simplified equations yields the following homogeneous relationships:

$$m\ddot{u}_{xC} + k_s u_{xC} = 0, \tag{9}$$

$$m\ddot{u}_{yC} + k_s u_{yC} = 0. \tag{10}$$

The resolution for constants A_x and A_y is feasible when the characteristic equation is satisfied:

$$ms^2 + k_s = 0. \tag{11}$$

Upon satisfying this equation, the solutions for the complex constant s pinpoint the undamped natural frequency of the shaft:

$$s_{1,2} = \pm i\omega_n, \tag{12}$$

where ω_n is the shaft's undamped natural frequency:

$$\omega_n = \sqrt{\frac{k_s}{m}} = \sqrt{\frac{48EI}{L^3 m}}. \tag{13}$$

The equation of motion, therefore, details undamped oscillatory motion at frequency $\pm\omega_n$. The undamped system's critical speed is:

$$\omega_{cr} = \pm\omega_n, \tag{14}$$

reflecting the lateral vibrations in both forward ($+\omega_n$) and backward ($-\omega_n$) directions.

Finally, the complete solutions to the undamped free vibration are expressed as a linear amalgamation of two individual solutions:

$$u_{xC} = B_{x1}\cos(\omega_n t) + B_{x2}\sin(\omega_n t), \tag{15}$$

$$u_{yC} = B_{y1}\cos(\omega_n t) + B_{y2}\sin(\omega_n t), \tag{16}$$

with B_{xi} and B_{yi} (i = 1, 2) as the coefficients determined by the initial conditions of the rotor [1].

2.2.2 Damped Free Vibration

Consideration of the Föppl/Jeffcott rotor's vibration analysis reveals the presence of measurable damping within the shaft, whilst imbalances are disregarded. This adjustment alters the previously stated motion equations by incorporating damping coefficients, which results in a modified set of equations for both the x and y axes.

$$m\ddot{u}_{xC} + k_s u_{xC} + c_s \dot{u}_{xC} = 0, \tag{17}$$

$$m\ddot{u}_{yC} + k_s u_{yC} + c_s \dot{u}_{yC} = 0. \tag{18}$$

The homogeneous second-order differential equations for the system with damping bear resemblance to the undamped system equations. Implementing the damped system's solutions into these equations yields a homogeneous equation set.

$$(ms^2 + k_s + c_s)A_x e^{st} = 0, \tag{19}$$

$$(ms^2 + k_s + c_s)A_y e^{st} = 0. \tag{20}$$

These are applicable under all initial conditions given that the damped characteristic equation is satisfied:

$$ms^2 + k_s + c_s = 0. \tag{21}$$

The damped characteristic equation's roots, or the damped eigenvalues of the system, are identified as:

$$s_{1,2} = -\frac{c_s}{2m} \pm j\sqrt{\frac{k_s}{m} - \left(\frac{c_s}{2m}\right)^2}. \tag{22}$$

The system is typically underdamped, indicated by the inequality:

$$\frac{c_s}{2m} < \sqrt{\frac{k_s}{m}}, \tag{23}$$

and s will have an imaginary component. The damping ratio is characterized as:

$$\xi = \frac{c_s}{2m\omega_n}. \tag{24}$$

This ratio equates to the system's effective damping c_s over the critical value for the damping constant at which the system becomes overdamped. Employing this ratio into the characteristic equation allows for the reformulation of the solutions:

$$s_{1,2} = -\xi\omega_n \pm j\omega_n\sqrt{1-\xi^2}. \tag{25}$$

The damped natural frequency, an integral part of $s_{1,2}$, is described as:

$$\omega_d = \omega_n\sqrt{1-\xi^2}. \tag{26}$$

The damped system exhibits oscillatory motion with these characteristics, where the frequency is dictated by the damped natural frequency ω_d. The damping leads to a gradual decrease in the oscillation's magnitude over time [1].

2.2.3 Forced Steady State Response

The final consideration in the analysis of the Föppl/Jeffcott rotor's forced reaction involves accounting for evident shaft damping yet excluding mass eccentricity. The motion's equations are redefined, incorporating the undamped natural frequency and damping ratio.

$$\ddot{u}_{xC} + 2\xi\omega_n\dot{u}_{xC} + \omega_n^2 u_{xC} = e_u\omega^2\cos(\omega t), \tag{27}$$

$$\ddot{u}_{yC} + 2\xi\omega_n\dot{u}_{yC} + \omega_n^2 u_{yC} = e_u\omega^2\sin(\omega t). \tag{28}$$

We amalgamate the rotor's x and y displacements into a singular complex coordinate for simplification:

$$u_C = u_{xC} + ju_{yC}, \tag{29}$$

which symbolizes the complex plane displacement of the rotor's disk center.

The steady-state response of the system is presumed to adopt a complex exponential form:

$$u_{xC} = U_x e^{j\omega t}, \tag{30}$$

$$u_{yC} = U_y e^{j\omega t}. \tag{31}$$

These solutions, upon application into the reformulated motion equations, culminate in a set of outcomes that intertwine the undamped natural frequency with the damping ratio. The unified complex exponential form emerges as:

$$u_C = U_x e^{j\omega t} + jU_y e^{j\omega t}. \tag{32}$$

Simplifying the above expression yields a single complex number that describes the rotor displacement:

$$u_C = Ue^{j\omega t}, \tag{33}$$

where U is defined as

$$U = U_x + jU_y. \tag{34}$$

Substituting the set of solutions back into the motion equations, we get:

$$(-\omega^2 + 2j\xi\omega_n\omega + \omega_n^2)U_x e^{j\omega t} = e_u\omega^2\cos(\omega t), \tag{35}$$

$$(-\omega^2 + 2j\xi\omega_n\omega + \omega_n^2)U_y e^{j\omega t} = e_u\omega^2\sin(\omega t). \tag{36}$$

The x and y-axis displacement equations are subsequently combined into the complex form by multiplying the sine component by j and adding it to the cosine component equation, resulting in a singular complex equation of motion:

$$(-\omega^2 + 2j\xi\omega_n\omega + \omega_n^2)U = e_u\omega^2. \tag{37}$$

The relationship between the displacement of the disk center in complex form and the non-zero mass eccentricity is considered to be a simple complex number ratio. This relationship can be computed from Eq. (37):

$$\frac{u_C}{e_u} = \frac{f_r^2}{[1 - f_r^2 + 2j\xi f_r]}, \tag{38}$$

where the frequency ratio f_r is defined as

$$f_r = \frac{\omega}{\omega_n}. \tag{39}$$

This ratio provides a non-time-dependent relationship. The solution in complex form can be expressed as a magnitude and phase shift:

$$\frac{u_C}{e_u} = \frac{|U|/e_u e^{-j\phi}}{\sqrt{(1 - f_r^2)^2 + (2\xi f_r)^2}}. \tag{40}$$

The dimensionless amplitude ratio of the forced response is

$$\left|\frac{U}{e_u}\right| = \frac{f_r^2}{\sqrt{(1 - f_r^2)^2 + (2\xi f_r)^2}}. \tag{41}$$

At the critical speed where $f_r = 1$, the amplitude ratio simplifies to:

$$\left|\frac{U}{e_u}\right| = \frac{1}{2\xi}. \tag{42}$$

With a low damping ratio, the amplitude ratio surges near the resonance frequency. For larger damping ratios, the resonance peak is muted. When f_r significantly exceeds 1, the amplitude of vibration nears unity [1].

The phase difference ϕ varies with the frequency ratio and is calculated as:

$$\phi = \tan^{-1}\left(\frac{2\xi f_r}{1 - f_r^2}\right). \tag{43}$$

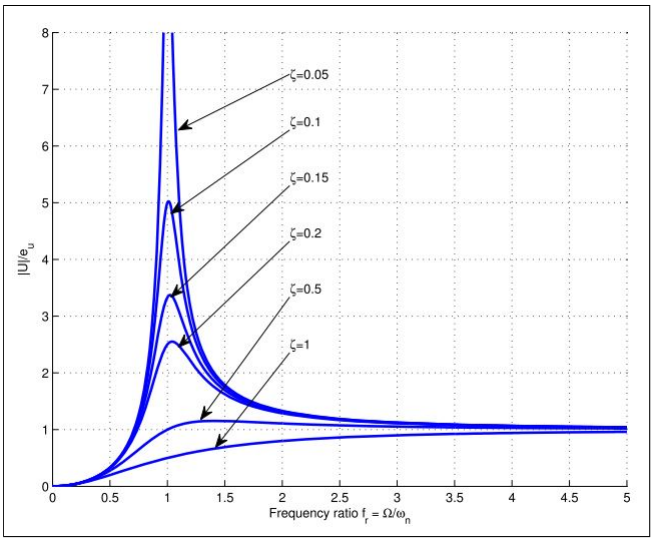

Figure 3: Amplitude of Forced Response for a Jeffcott Rotor vs. Frequency Rotor [1]

For very low frequencies, the amplitude ratio is negligible, reflecting the small impact of unbalanced forces. As frequency increases, there's a prominent peak in amplitude at resonance. Finally, for high frequencies beyond resonance, the amplitude ratio approaches unity and the phase angle nears 180 degrees, indicating that the center of gravity of the disk is following an orbit drawn by the geometric center in opposition to the inertial forces of the rotor [1].

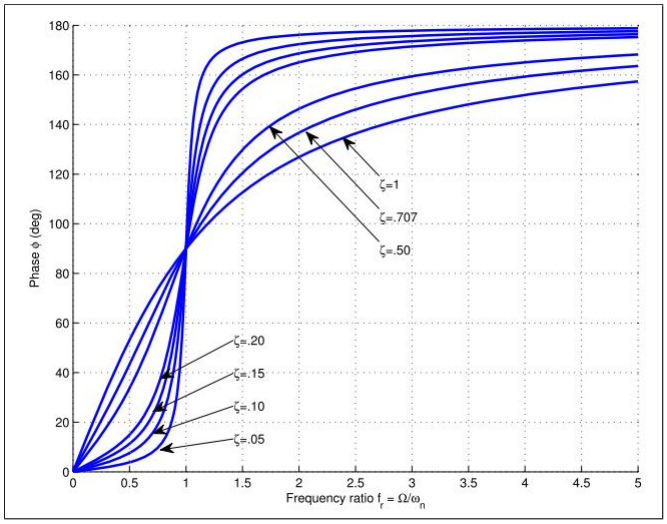

Figure 4: Phase angle Φ of Forced Response for a Jeffcott Rotor vs. Frequency Ratio [1]

2.3 Rotor Gyroscopic Effects

Gyroscopic effects on rotor systems equipped with flexible bearings must be understood in order to conduct a detailed analysis of rotor bearings. This will build upon the Föppl/Jeffcott rotor model discussed previously, where we initially considered a system with rigid bearings that ensured alignment of the shaft axis with the bearing centerline, thereby neglecting inertia-induced moments [1].

By analyzing a cylindrical rotor on flexible bearings, we can deduce the undamped free vibration and the rotor's natural frequency as influenced by shaft speed. The findings aim to reveal the critical speed's dependence on rotor geometry and rotation rate, emphasizing the significant impact of gyroscopic forces. These forces, inherently linked to the rotor's angle of tilt, angular inertia, and shaft speed, not only fuse the lateral movements along the horizontal and vertical axes, affecting one another reciprocally but also modulate the critical speeds away from initial zero-speed estimates. As we venture deeper into the gyroscopic dynamics, we'll uncover how these moments can either escalate or reduce the critical speeds for certain system modes, variably determined by the rotational velocity [1].

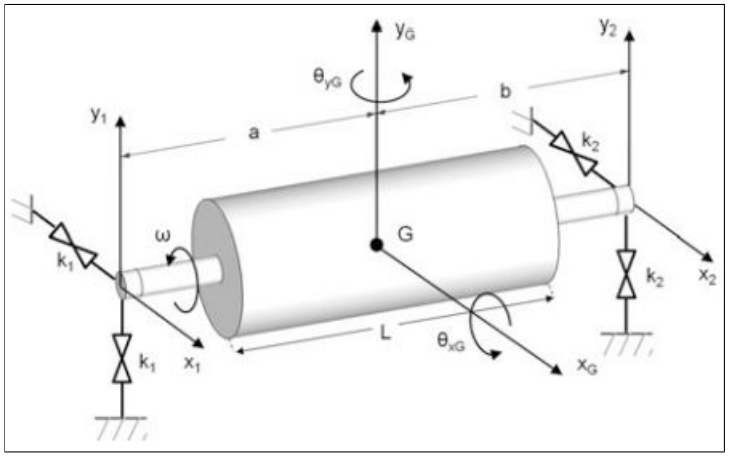

Figure 5: Example of a Cylindrical Rotor w/ Isotropic Symmetric Flexible Bearings [1]

2.3.1 Rigid Circular Rotor on Flexible Undamped Bearings

A rigid rotor, as seen in Figure 5, can be characterized by its cylindrical form, with a mass m, length L, and operational angular velocity ω. The rotor is supported by bearings that offer lateral flexibility, quantified by stiffness coefficients k_1 and k_2. The bearings' axial distances from the rotor's center of gravity, G, are denoted as a for the left and b for the right, and the complete distance between them is L_b. Disregarding the shaft's mass, the rotor's polar moment of inertia is calculated as:

$$J_p = \frac{mR^2}{2}, \tag{44}$$

where R is the radius of the rotor. This value signifies the rotational inertia of the cylindrical mass with respect to its principal rotation axis. Meanwhile, the transverse moment of inertia is given by:

$$J_t = \frac{m}{4}\left(R^2 + \frac{1}{3}L^2\right), \tag{45}$$

reflecting the inertia about an axis that runs perpendicular to the main axis of rotation. A pivotal parameter in subsequent discussions is the ratio P of the polar to the transverse moment of inertia, formulated as:

$$P = \frac{J_p}{J_t} = \frac{2}{1 + \frac{1}{3}\left(\frac{L}{R}\right)^2}. \tag{46}$$

This ratio, P, is significantly influenced by the rotor's geometric configuration. When the rotor's radius is substantially greater than its length ($R \gg L$), the inertia ratio gravitates towards $P \approx 2$. In contrast, for slender rotors where the radius is relatively small in comparison to the length ($R \ll L$), the ratio leans towards infinity, causing P to approximate zero. When the ratio of the rotor's length to its radius is equal to $\sqrt{3}$, P is equal to one, showcasing the direct correlation between the rotor's geometrical attributes and its inertial properties [1].

2.3.2 Modeling a Rigid Circular Rotor with Gyroscopic Moments

The analysis of a rigid cylindrical rotor, as depicted in Figure 5, involves a rotor characterized by its mass, length, and angular velocity, and supported by flexible bearings with defined lateral stiffness. Lateral displacements and rotations around the rotor's center of mass occur in the x and y directions, with the rotation at the center of mass about the x-axis denoted as θ_{xG} and about the y-axis as θ_{yG}. These can be quantified by:

$$x_G = \frac{1}{L_b}(bx_1 + ax_2), \tag{47}$$

$$y_G = \frac{1}{L_b}(by_1 + ay_2), \tag{48}$$

$$\theta_{xG} \approx \frac{1}{L_b}(y_2 - y_1), \tag{49}$$

$$\theta_{yG} \approx \frac{1}{L_b}(x_2 - x_1), \tag{50}$$

where x_1 and y_1 are the lateral displacements of the shaft at the first bearing location, and x_2 and y_2 are the displacements at the second bearing location, as shown in Figure 5.

The equations explaining the motion for the translation and rotation of the rotor about its center of mass are given by

$$m\ddot{x}_G + \alpha x_G - \gamma \dot{y}_G = 0, \tag{51}$$

$$m\ddot{y}_G + \alpha y_G + \gamma \dot{x}_G = 0, \tag{52}$$

$$J_t\ddot{\theta}_{xG} + J_p\dot{\theta}_{yG} + \gamma x_G + \delta\theta_{xG} = 0, \tag{53}$$

$$J_t\ddot{\theta}_{yG} - J_p\dot{\theta}_{xG} + \gamma y_G + \delta\theta_{yG} = 0, \tag{54}$$

where the stiffness parameters α, γ, and δ are defined as:

$$\alpha = k_1 + k_2, \tag{55}$$

$$\gamma = -k_1 a + k_2 b, \tag{56}$$

$$\delta = k_1 a^2 + k_2 b^2 \tag{57}$$

The dynamic behavior of a rigid cylindrical rotor is captured by a set of equations that segregate translational motion from angular dynamics. The first pair of equations pertain to lateral motion, while the latter pair govern angular movements. The equations incorporate a linearized gyroscopic term which influences the rotational dynamics along the x-axis and y-axis, relevant for scenarios involving small amplitude oscillations as detailed in the referenced studies. A notable feature of these dynamic equations is the potential for decoupling the translational motion from angular motion when the coupling parameter γ is null, allowing for independent resolution of these motions [1].

$$m\ddot{x}_G + \alpha x_G - \gamma \dot{y}_G = 0, \tag{58}$$

$$m\ddot{y}_G + \alpha y_G + \gamma \dot{x}_G = 0, \tag{59}$$

$$J_t\ddot{\theta}_{xG} + J_p\dot{\theta}_{yG} + \gamma x_G + \delta\theta_{xG} = 0, \tag{60}$$

$$J_t\ddot{\theta}_{yG} - J_p\dot{\theta}_{xG} + \gamma y_G + \delta\theta_{yG} = 0. \tag{61}$$

The aforementioned dynamic equations are elegantly expressed in vector form as:

$$M\ddot{X} + \omega G\dot{X} + KX = 0, \tag{62}$$

where the state vector is defined by:

$$X = \begin{bmatrix} x_G \\ y_G \\ \theta_{xG} \\ \theta_{yG} \end{bmatrix}, \tag{63}$$

and the matrices for mass (M), gyroscopic effects (G), and system stiffness (K) are given by:

$$M = \begin{bmatrix} m & 0 & 0 & 0 \\ 0 & m & 0 & 0 \\ 0 & 0 & J_t & 0 \\ 0 & 0 & 0 & J_t \end{bmatrix}, \tag{64}$$

$$G = \begin{bmatrix} 0 & 0 & 0 & 0 \\ 0 & 0 & 0 & 0 \\ 0 & 0 & 0 & J_p \\ 0 & 0 & -J_p & 0 \end{bmatrix}, \tag{65}$$

$$K = \begin{bmatrix} \alpha & 0 & 0 & \gamma \\ 0 & \alpha & -\gamma & 0 \\ 0 & \gamma & \delta & 0 \\ -\gamma & 0 & 0 & \delta \end{bmatrix}. \tag{66}$$

By assuming the stiffness of all support bearings is the same and the rotor is axially symmetrical about its center of mass, the equations of motion can be decoupled, simplifying the analysis:

$$K = \begin{bmatrix} \alpha & 0 & 0 & 0 \\ 0 & \alpha & 0 & 0 \\ 0 & 0 & \delta & 0 \\ 0 & 0 & 0 & \delta \end{bmatrix} \tag{67}$$

2.3.3 Undamped Natural Frequencies of the Cylindrical Mode

The resolution of the rotor's dynamics is described by the translational motion Eq.s (60) and (61). We consider the system's homogeneous linear differential equations to exhibit complex exponential solutions:

$$x_G = U_{xG}e^{st}, \tag{68}$$

$$y_G = U_{yG}e^{st}. \tag{69}$$

Subsequent to integrating these solutions into the motion equations, what remains is the following:

$$(ms^2 + \alpha)U_{xG} = 0, \tag{70}$$

$$(ms^2 + \alpha)U_{yG} = 0. \tag{71}$$

The encapsulated expressions within parentheses serve as the characteristic polynomial, with the roots of the characteristic Eq. (72) determining the system's natural frequencies:

$$ms^2 + \alpha = 0, \tag{72}$$

$$s = \pm j\omega_n. \tag{73}$$

The eigenvalues connected to the horizontal and vertical axes are identical and uncoupled, as anticipated due to the absence of lateral translation contributing to rotor tilt, and thus a nullified gyroscopic moment. The undamped natural frequencies for the cylindrical mode, delineated as forward and backward modes, are derived as:

$$\omega_{n1} = \omega_{n3} = \sqrt{\frac{2k}{m}}, \tag{74}$$

$$\omega_{n2} = \omega_{n4} = -\sqrt{\frac{2k}{m}}. \tag{75}$$

2.3.4 Undamped Natural Frequencies of the Conical Mode

Moving onto the angular dynamics of the rotor, following Eq.s 61 and 62, an assumption that the solutions to the homogeneous system can be made in a complex exponential form:

$$\theta_{xG} = \Theta_{xG}e^{st}, \tag{76}$$

$$\theta_{yG} = \Theta_{yG}e^{st}. \tag{77}$$

These constants Θ_{xG} and Θ_{yG} are substituted back into the equations, yielding a homogeneous equation system:

$$(J_t s^2 + \delta)\Theta_{xG} + J_p \omega s \Theta_{yG} = 0, \tag{78}$$

$$(J_t s^2 + \delta)\Theta_{yG} - J_p \omega s \Theta_{xG} = 0. \tag{79}$$

The characteristic equation derived from these equations is formulated by setting the determinant of the system matrix to zero:

$$\det \begin{bmatrix} J_t s^2 + \delta & J_p \omega s \\ -J_p \omega s & J_t s^2 + \delta \end{bmatrix} = 0. \tag{80}$$

This characteristic equation conveys that the angular dynamics around the distinct lateral axes are coupled through the gyroscopic moments, with the rotor's rotational speed significantly influencing the natural frequencies corresponding to the rotor's conical mode [1].

A special case is the conical mode at zero rotating speed; in which case, the non-rotating conical natural frequency is

$$\omega_{nC0} = \sqrt{\frac{kL_b^2}{2J_t}} \tag{81}$$

In the general case, with non-zero rotating speeds, the natural frequencies of the rotor's conical modes can be classified into lower and higher frequencies, stemming from the roots of Eq. (2.67). Frequencies for the dimensionless lower mode's forward component $\tilde{\omega}_{n3}$, and the higher mode's backward component $\tilde{\omega}_{n8}$, are given by:

$$\tilde{\omega}_{n5} = -Pf_{rco}/2 + \sqrt{(Pf_{rco}/2)^2 + 1}, \tag{82}$$

$$\tilde{\omega}_{n8} = -Pf_{rco}/2 - \sqrt{(Pf_{rco}/2)^2 + 1}. \tag{83}$$

The lower mode's backward component $\tilde{\omega}_{n6}$, and the higher mode's forward component $\tilde{\omega}_{n7}$:

$$\tilde{\omega}_{n6} = Pf_{rco}/2 - \sqrt{(Pf_{rco}/2)^2 + 1}, \tag{84}$$

$$\tilde{\omega}_{n7} = Pf_{rco}/2 + \sqrt{(Pf_{rco}/2)^2 + 1}. \tag{85}$$

These dimensionless frequencies characterize the rotor's forward and backward conical modes [1].

2.4 Instability via Aerodynamic Cross-Coupling

In rotor dynamic systems, such as in turbines in TGs, cross-coupling forces often emerge as a primary source of instability. These forces arise from aerodynamic interactions within uneven clearances of impellers and seals, exacerbated by lateral rotor movements. Traditional systems employing fluid-film bearings are notably susceptible, as the rotor may not be centrally aligned, increasing the likelihood of whirling motions. Such disturbances can precipitate significant vibrations and, with increasing pressure in components like compressors, lead to a critical reduction in damping—especially at speeds near the first critical speed. This scenario is particularly precarious when these forces act near the rotor's midspan, away from the stabilizing influence of bearings, culminating in system instability in TGs and propulsion mechanisms.

2.4.1 Aerodynamic Cross-Coupling in Turbines

Forces that tend to destabilize the turbine wheel, known as Alford forces or aerodynamic cross-coupling forces, interconnect the rotor's lateral axes of motion through stiffness values. Assuming the rotor's displacements at a turbine stage are x_d and y_d, the cross-coupling forces are mathematically represented by:

$$\begin{bmatrix} F_{d_x} \\ F_{d_y} \end{bmatrix} = \begin{bmatrix} q_{sxx} & q_{sxy} \\ q_{syx} & q_{syy} \end{bmatrix} \begin{bmatrix} x_d \\ y_d \end{bmatrix}, \tag{86}$$

where F_{d_x} and F_{d_y} are the resulting forces, and q_{sxx}, q_{syy}, q_{sxy}, and q_{syx} correspond to stiffness coefficients.

In practice, it is observed that the primary aerodynamic stiffness values are less significant compared to the cross-coupling coefficients, allowing for the expression of cross-coupling forces to be simplified to:

$$\begin{bmatrix} F_{s_x} \\ F_{s_y} \end{bmatrix} = \begin{bmatrix} 0 & -q_a \\ q_a & 0 \end{bmatrix} \begin{bmatrix} x_d \\ y_d \end{bmatrix}, \tag{87}$$

using a singular cross-coupling stiffness coefficient q_a, which Alford estimated for a turbine stage as:

$$q_a = \frac{T\beta}{D_m L_t}, \tag{88}$$

with T as the torque on the turbine stage, β as a correction factor, D_m as the mean blade diameter, and L_t as the blade radial length. Alford proposed a value range for β based on empirical data from aircraft gas turbines [1].

2.5 Lateral Vibration Analysis

The critical speed of a rotor occurs when its operating speed induces periodic excitation forces that match the system's natural frequency, including the rotor, bearings, and supports. Typically, attention is focused on the lateral critical speed, which arises from the interplay between the rotor's lateral vibrational frequency and the bearings' stiffness and damping characteristics. Nowadays, high-performance machinery often operates above the first critical speed [3].

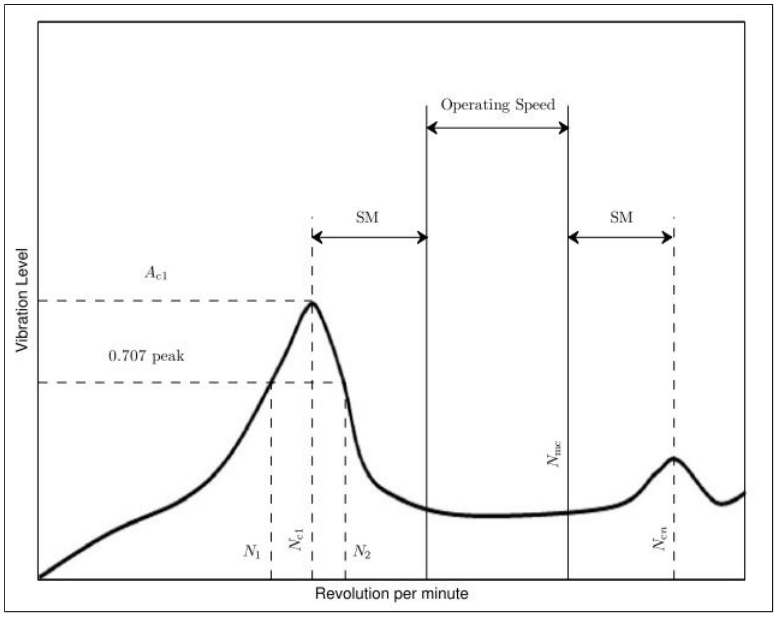

Figure 6: Theoretical Forced Response of a Rotor [1]

Figure 6 describes the amplitude of lateral vibration against rotational speed for a typical rotor-dynamic system, marking each critical speed N_{ci} at the respective vibrational response peaks, with amplitude A_{ci}. The Amplification Factor (AF) is calculated by the ratio of the first critical speed N_{ci} to the range of speeds beyond half the peak amplitude's power, $N_2 - N_1$. Additionally, the system's Maximum continuous operating speed (MCOS), denoted as N_{mc}, is set at 105% of the machine's top-rated speed. The speeds between N_{mc} and the lowest operational speed define the machine's operational range. The Separation Margin (SM) is another crucial metric in this context [5].

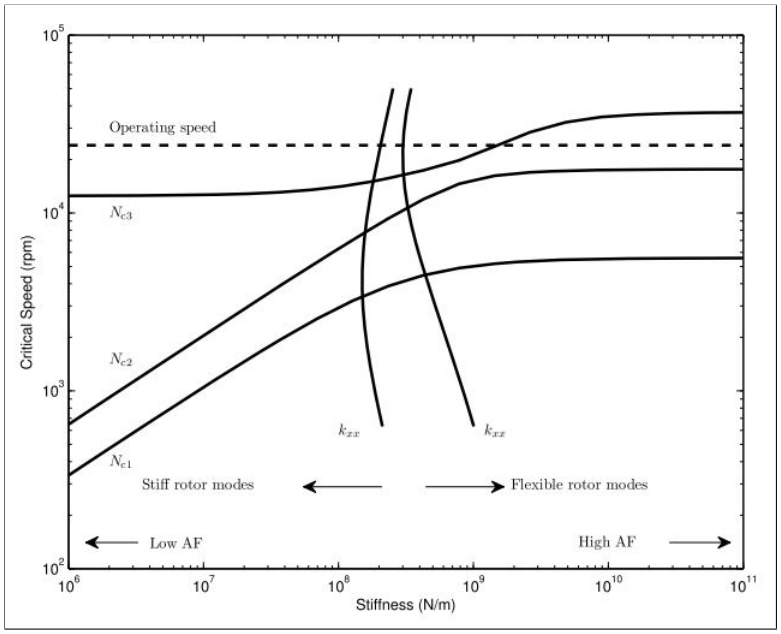

Figure 7: Undamped Critical Speed vs. Stiffness map [1]

Disturbances in rotor-dynamic systems are often tied to the mechanical and electrical aspects of the machinery and can be mitigated during the design phase or with proper maintenance. In the analysis of lateral vibrations, the forced response due to rotor imbalance is of primary focus, while the influence of cross-coupling forces will be explored in a subsequent discussion on rotor stability [1].

For lateral vibration analysis, the initial phase typically involves the determination of the rotor-dynamic system's critical speeds and mode shapes, up to 125% of the Maximum Continuous Operating Speed (MCOS). This involves constructing an undamped critical speed map and overlaying the computed stiffness of the system supports in both the horizontal (k_{xx}) and vertical (k_{yy}) directions, as depicted in Figure 7.

2.6 Finite Element Modeling of a Rotor

In the realm of rotor-dynamic systems, particularly within TG propulsion units, the bearings play a critical role, primarily concerning the lateral dynamics of the rotor. While axial vibrations warrant attention for potential issues, it is the lateral vibrations that commonly

signal instability in such machines. An exacting model of lateral dynamics is paramount for the evaluative and testing processes integral to the design and operational phases of TG turbine elements. This need for precision in modeling is even more pronounced with AMBs, given their pivotal role in stabilizing inherently unstable bearing systems, and thus necessitating dependable, model-based controllers for routine functionality.

For flexible rotors like those used in TG turbines, lateral dynamics are governed by complex partial differential equations with spatially distributed parameters, which often preclude analytical solutions, especially for rotors with intricate geometries. A pragmatic approach in real-world scenarios, such as within TG systems, is the use of a linearized model that approximates lateral dynamics, which suffices for most analytical and design purposes. Such methodologies underpin the design of robust controllers for AMBs. The employment of the Finite Element Method (FEM) is a common strategy in these contexts. FEM simplifies the rotor's continuous spatial domain to a discrete system, defined by a finite set of degrees of freedom associated with shaft elements, thus streamlining the complex spatial variables present in the original beam equations.

This section will detail the finite element modeling process required for simulating elements like turbine components in TG systems.

2.6.1 Discretizing Rotor into Finite Elements

To construct a finite element model, the rotor is segmented along its length into uniform beam elements, each flanked by node points, as displayed in Figure 8, where nodes appear as darkened dots. For an effective mesh that truly represents the rotor's properties, several guidelines rooted in the rotor's structure and the placement of key components—such as disks, bearings, and other elements—are followed [7].

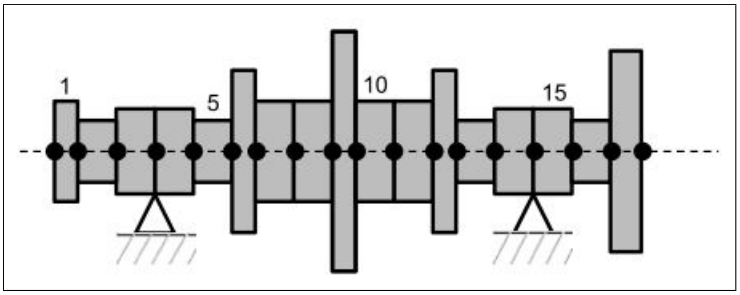

Figure 8: Example Discretized Rotor Mesh [1]

Initially, a node is situated at every point along the rotor where a change in diameter occurs, ensuring all shaft elements share a consistent radius, which simplifies subsequent dynamic modeling of each element. Additionally, nodes are allocated at points where mass/inertia disks, bearings, seals, or any external forces act, centralizing these influences at discrete points along the rotor. This approach also aggregates all sensor measurements and other relevant data points at the node points, streamlining the input and output variable definition in the finite element model's formulation. To maintain model accuracy, the element's length-to-diameter ratio should be approximately one or smaller [7].

2.6.2 Approximation of Element and Nodal Displacement

The investigation into rotor dynamics begins with partitioning the shaft into smaller subdivisions, each evaluated independently. Each subdivision's dynamics are characterized by nodal degrees of freedom that encapsulate both displacements and rotations, as depicted in Figure 9. For the sake of simplicity in examining lateral dynamics, each subdivision is accorded eight degrees of freedom—accounting for two displacements and two rotations at each node.

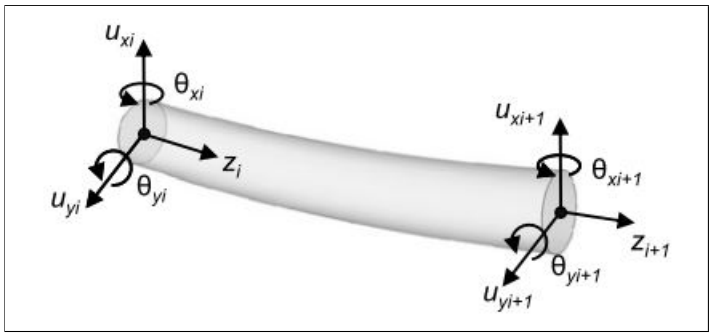

Figure 9: Generalized Displacements in a Beam Element [1]

The displacements at the i-th node in the horizontal and vertical axes are denoted by u_{xi} and u_{yi}, respectively. The angular displacements around the y and x axes at the same node are expressed as

$$\theta_{yi} = \frac{\partial u_{xi}}{\partial z}, \tag{89}$$

and

$$\theta_{xi} = \frac{\partial u_{yi}}{\partial z}. \tag{90}$$

The degrees of freedom at the i-th node are assembled into the generalized displacement vector q_i, which describes the node's position and rotation at any given moment. This vector is configured as

$$q_i = \begin{bmatrix} u_{xi} \\ u_{yi} \\ \theta_{yi} \\ \theta_{xi} \end{bmatrix}. \tag{91}$$

The generalized displacement of the i-th shaft segment amalgamates the displacement vectors at its end nodes q_i and q_{i+1}, forming the generalized displacement vector for the segment as illustrated in Figure 9:

$$Q_i = \begin{bmatrix} q_i \\ q_{i+1} \end{bmatrix}. \tag{92}$$

This generalized displacement vector is pivotal in deducing the entire shaft segment's state within the dynamic model. The eight components of Q_i distinctly delineate the shape of the i-th beam segment in the finite element framework.

Employing the degrees of freedom at the rotor mesh, we interpolate the lateral displacement and rotation along any point of the shaft segment. The segment's contour is estimated

with the generalized displacement vector Q_i and the established shape functions N_j. These shape functions, cubic in nature for the shaft element, are presented as

$$N_1 = \frac{1}{L^3}\left(L^3 - 3Lz^2 + 2z^3\right), \tag{93}$$

$$N_2 = \frac{1}{L^2}\left(zL^2 - 2Lz^2 + z^3\right), \tag{94}$$

$$N_3 = \frac{1}{L^3}\left(3Lz^2 - 2z^3\right), \tag{95}$$

$$N_4 = \frac{1}{L^2}\left(-zL^2 + z^3\right). \tag{96}$$

where L denotes the length of the shaft segment and z the axial position.

With the set of shape functions defined from Eq.s 93 to 96, the lateral translation of the i-th shaft segment at any axial position z and time t is expressed as a function of time and the axial offset from the leftmost node:

$$\begin{bmatrix} u_{xi}(z,t) \\ u_{yi}(z,t) \end{bmatrix} = \begin{bmatrix} N_1 & 0 & N_2 & 0 & N_3 & 0 & N_4 & 0 \\ 0 & N_1 & 0 & -N_2 & 0 & N_3 & 0 & -N_4 \end{bmatrix} Q_i. \tag{97}$$

In the same vein, the lateral rotations $\theta_{yi}(z,t)$ and $\theta_{xi}(z,t)$ at any axial position z are derived by computing the partial derivatives of the above with respect to z.

A noteworthy insight from Eq. 97 is the inclusion of the spatial variable z in the matrix of basis functions, whereas the generalized displacement vector Q_i is time-dependent. Hence, the finite element approach condenses the dynamic characterization of the original continuous shaft element to a finite quantity of degrees of freedom, effectively rendering it as a discrete shaft system [6].

2.6.3 Equations of Motion Describing Each Element

The equation of motion for each section of the shaft is established via the Lagrange formulation, leading to:

$$\frac{d}{dt}\left(\frac{\partial \mathcal{L}_i}{\partial \dot{q}_i}\right) - \frac{\partial \mathcal{L}_i}{\partial q_i} + \frac{\partial R_i}{\partial \dot{q}_i} = 0. \tag{98}$$

The Lagrangian, represented as $\mathcal{L}_i$, for a shaft segment, is the resultant of its kinetic energy T_i and potential energy U_i, given by:

$$\mathcal{L}_i = T_i - U_i. \tag{99}$$

In this system, R_i characterizes the energy loss due to internal damping, referred to as the dissipation function. When the generalized displacement of a shaft element is modeled as detailed in Eq. 97, the kinetic and potential energy expressions are readily obtainable through classical beam theories such as Bernoulli-Euler or Timoshenko. The potential energy largely stems from the effects of beam bending and shear, while the kinetic energy is influenced by both the lateral and rotational inertial dynamics of the shaft segment.

Integrating the energy expressions into Eq. (2.93) and considering the dynamics of a singular shaft section, we arrive at the lateral dynamics described in the ensuing vector differential equation:

$$M_i\ddot{Q}_i + C_i\dot{Q}_i + G_i\dot{Q}_i + K_iQ_i = F_i. \tag{100}$$

Within this framework, M_i corresponds to the mass matrix, C_i to the damping matrix, G_i to the gyroscopic matrix, K_i to the stiffness matrix, and F_i to the applied external force vector. The finite element method's objective is to derive the expressions for these system matrices from Lagrange's equations of motion and the generalized displacement vectors outlined in Eq. 97.

2.6.4 Element Mass and Gyroscopic Matrices

The kinetic energy for a segment within a rotor mesh is attributed to both its translational and rotational motion. Considering a segment characterized by the generalized displacement detailed in Eq. (2.92), the kinetic energy takes the form:

$$T_i = \frac{1}{2}\dot{Q}_i^T M_i \dot{Q}_i + \frac{1}{2}\omega Q_i^T W_i Q_i. \tag{101}$$

The mass matrix M_i and the matrix W_i, associated with the segment's polar moment of inertia and affected by the rotational speed ω, are essential in this formulation. The methodologies for calculating these matrices are available in specialized texts.

The influence of kinetic energy in the Lagrange equation is manifested in the initial two terms of Eq. (2.93). Specifically, the first term representing the kinetic energy is expressed as:

$$\frac{d}{dt}\left(\frac{\partial T}{\partial \dot{Q}_i}\right) = M_i \dot{Q}_i + \frac{1}{2}\omega W_i Q_i. \tag{102}$$

Furthermore, the second kinetic term within the Lagrange equation is presented as:

$$-\frac{\partial T}{\partial Q_i} = -\frac{1}{2}\omega^2 W_i^T Q_i. \tag{103}$$

When these kinetic terms are integrated, we obtain the complete kinetic contribution within the Lagrange framework:

$$\frac{d}{dt}\left(\frac{\partial T}{\partial \dot{Q}_i}\right) - \frac{\partial T}{\partial Q_i} = M_i \dot{Q}_i + \frac{1}{2}\omega(W_i - W_i^T)Q_i = M_i \dot{Q}_i + G_i Q_i. \tag{104}$$

Here, G_i is identified as the gyroscopic matrix, derived from W_i and the rotational speed ω.

Documentation for the matrices M_i and G_i for uniform segments is readily available. These matrices, dependent on the segment's dimensions and material properties, are standard across the mesh, facilitating automated calculations, and assuming proper initial setup.

2.6.5 Element Stiffness Matrix

Rooted in the Bernoulli–Euler beam theory, the potential energy for a segment of a rotor mesh is primarily sourced from the internal strain energy due to lateral bending. This energy for an element with generalized displacements is formulated as:

$$U_i = \frac{1}{2}Q_i^T K_i Q_i. \tag{105}$$

The matrix K_i, known as the stiffness matrix, encapsulates the axial strain/stress response characteristics attributable to the lateral bending of the beam segment. The methodology for calculating K_i is detailed in referenced scholarly articles.

Subsequent to the derivation of the potential energy, it is utilized in the second term of the Lagrange equation as shown in Eq. (93), resulting in:

$$\frac{\partial U_i}{\partial Q_i} = K_i Q_i. \tag{106}$$

The coefficients within the stiffness matrix K_i are elaborated in designated references, linked to attributes such as the element's length, cross-sectional area, moment of inertia, and modulus of elasticity. The computation of the stiffness matrix for all shaft segments, akin to the mass and gyroscopic matrices, can be automated effectively, assuming detailed rotor mesh information is at hand [4].

2.6.6 Element Damping Matrix

The dissipation of energy in the shaft due to internal friction is generally minimal, hence the dissipation function is often neglected in finite element models. However, for scenarios where dissipation is significant, the expression for R_i is:

$$R_i = \frac{1}{2}\dot{Q}_i^T C_i \dot{Q}_i, \tag{107}$$

where C_i represents the damping matrix of the shaft segment.

Integrating this dissipation function into the Lagrange equation (Eq. 2.93), the third term is formulated as:

$$\frac{\partial R_i}{\partial \dot{Q}_i} = C_i \dot{Q}_i. \tag{108}$$

Combining the terms from the Lagrange equation pertaining to the kinetic energy (Eq. 99), potential energy (Eq. 101), and the dissipation function (Eq. 103), we derive the vector differential equation for the shaft segment as described in Eq. (95) [4].

2.6.7 Introduction of Lumped Mass, Stiffness and Damping Components

Complex rotor designs may incorporate impellers, motor cores, and other mass disks that impact the dynamics of the rotor/support system. These elements are modeled as rigid disks at specific shaft nodes, with their respective masses and moments of inertia added to the shaft model. Assuming the disk centers align with certain nodal points in the rotor mesh, the generalized displacement vector at the disk's node is defined as:

$$q_d = \begin{bmatrix} u_{xd} \\ u_{yd} \\ \theta_{yd} \\ \theta_{xd} \end{bmatrix}. \tag{109}$$

The vector differential equation for the disk takes the form:

$$M_d \ddot{q}_d + G_d \dot{q}_d = 0, \tag{110}$$

where M_d is the diagonal mass matrix of the disk, and G_d is the skew-symmetric gyroscopic matrix. Detailed expressions for these matrices are provided in Section 2.2.

Seals and bearings also play critical roles in rotor-dynamic systems by adding stiffness and damping at specific nodes. For a node corresponding to a bearing or seal, the generalized displacement vector q_b is used. The vector differential equation for stiffness and damping is:

$$C_b\dot{q}_b + K_b q_b = 0. \tag{111}$$

In this equation, C_b is the damping matrix, and K_b is the stiffness matrix of the bearing or seal. These matrices are typically provided by manufacturers and often depend on the shaft speed [4].

2.6.8 Assembly of the Global Mass, Gyroscopic, Stiffness, Damping Matrices, and Force Terms

Finally, the system matrices for the shaft, disks, and other components are assembled to form the global matrices. The global generalized displacement vector is defined as:

$$Q = [q_1\ q_2\ q_3\ \cdots\ q_{n+1}]^T, \tag{112}$$

The vector differential equation for the entire rotor-dynamic system is:

$$M\ddot{Q} + G\dot{Q} + C\dot{Q} + KQ = F, \tag{113}$$

where M is the global mass matrix, G the global gyroscopic matrix, C the global damping matrix, and K the global stiffness matrix. The generalized external force vector F encompasses all external disturbances affecting the system dynamics.

The system matrices in Eq. (108) are constructed by integrating the individual matrices from each shaft node, thus incorporating all components of the finite element model. The process for forming the global matrices is as follows: each element's mass matrix is integrated into the global mass matrix M. This involves summing the contributions of the mass, gyroscopic, damping, and stiffness matrices from each component into their respective global matrices [4].

3 Methodology and Execution

3.1 Overview

In developing a rotor dynamics analysis software suite using MATLAB, three fundamental aspects must be addressed: defining the model, forcing and operating conditions; analyzing the system and generating the results; and providing graphical means for interpreting the model and results. Each of these aspects is critical for ensuring the software's functionality, usability, and accuracy. The understanding of what/how features should be implemented was gathered through analyzing existing rotor dynamics analysis software suites.

3.2 Key Features

3.2.1 Analyzing a Model, Forcing, and Operating Conditions

The definition of the system, encompassing the model, forcing, and operating conditions, is crucial as it lays the foundation for all subsequent analysis and interpretation. Elements are incorporated into a single MATLAB structured array to facilitate the seamless passing of the model to various analysis or plotting functions. The rotating systems considered can be modeled in either the stationary or the rotating frame of reference. These systems would form the core of the software and offer a range of bearing options. The software should also have the capability for analyzing machines with asymmetric rotors, where the analysis can be performed in the rotating frame. Specific analysis functions, such as the time simulation of machines with non-linear fluid bearings, should also be available.

3.2.2 Model Interpretation - Graphical and Numerical Representation of Results

The final and most important of rotor dynamics analysis software is the graphical interpretation of the model and results. MATLAB's plotting and formatting facilities can be utilized to generate clear and informative visualizations. These graphical tools are essential for checking the model for any errors and for interpreting the results effectively. A key plot can be generated to verify the model, as any errors in the model definition are easily spotted through visual inspection. The software includes a variety of functions to support this, ensuring that users can validate and understand the model and its behavior comprehensively.

4 Cambridge Rotordynamics Software Suite

4.1 Overview

The Cambridge Rotorsol Suite is a dynamic rotor analysis software written in MATLAB that is specifically suitable for lateral vibration analysis. This software operates on a definition of a model and the forcing and operating conditions to analyze the system and generate results. It provides a graphical means for interpreting the model and results. The system's definition, which includes the model, forcing, and operating conditions, is combined into a single MATLAB structured array. This structured array, once established, facilitates the easy transfer of the model to analysis or plotting functions.

This suite can model rotating systems using a stationary or rotating frame of reference. It is possible to analyze machines with asymmetric rotors, where the analysis is conducted in the rotating frame, assuming isotropic bearings and stator. The software also has a plotting function to check the model and interpret results.

4.2 Defining the System

4.2.1 Defining Nodes

The nodes in the model are defined by their axial positions, as we are primarily concerned with shaft line models. Typically, nodes are numbered sequentially, though in the case of co-axial rotors, the nodes may not follow this sequence and their positions could overlap [8].

4.2.2 Shaft Elements

The shaft elements can be defined using either Euler or Timoshenko beam theories, applicable in both stationary and rotating frames. The shafts can be symmetric or asymmetric, with properties specified in different directions, and tapered shafts are also an option in the stationary frame. The main types of shaft elements include:

- Circular section shafts
- Asymmetric shafts
- Circular section tapered shafts

The damping factor provides proportional damping of the stiffness matrix for the element. The shaft type determines whether shear, rotary inertia, or gyroscopic effects are included in the analysis [8].

4.2.3 Disk Elements

Disks are defined using a similar structured array format, with different disk types specified by their properties. The types include [8]:

- Circular disks defined by dimensions and mass density.
- Disks specified by mass and moments of inertia.

- Circular disks without gyroscopic effects.
- Disks specified by mass and moments of inertia without gyroscopic effects.

4.2.4 Bearings, Seals, and Other Rotor-Stator Interactions

Bearings in the model are defined by their type and properties, which include rigid bearings, constant stiffness and damping, hydrodynamic short width bearings, and seals. The bearing types are [8]:

- Rigid short bearing - pinned boundary conditions
- Rigid long bearing - clamped boundary conditions
- Constant stiffness and damping - diagonal, no rotational stiffness
- Constant stiffness and damping - diagonal
- Constant stiffness and damping - no rotational stiffness - 2x2 matrices required
- Constant stiffness and damping - full 4x4 matrices required
- Hydrodynamic short width bearing theory
- Seals

4.2.5 Forcing Definition

The forcing elements in the model are defined based on the type of force applied. The force types include:

- Mass Unbalance
- Couple Unbalance
- Bent Shaft
- Foundation Excitation – frequency domain
- Foundation Excitation by a pulse – time domain
- Spinner Excitation through an Auxiliary Bearing

The structured approach to system definition in the Cambridge Rotorsol Suite allows for comprehensive and flexible modeling of rotor dynamics, accommodating various configurations and analysis requirements. This ensures accurate representation and analysis of complex rotor systems, providing valuable insights into their behavior and performance [8].

4.3 Features and Functions

The Cambridge Rotorsol Suite provides a range of analysis functions for rotor dynamics, each requiring the input of the model structured array and additional parameters such as rotor spin speed. These functions are designed to calculate various dynamic responses and characteristics of the rotor system. Below is a summary of the key features provided by these analysis functions.

- **Calculate Characteristic Roots and Modes (Eigenvalues and Eigenvectors)**
  The software can compute eigenvalues and eigenvectors at specified rotor speeds. This can be done for a single rotor speed or a vector of speeds, enabling the creation of natural frequency maps or Campbell diagrams. The output includes the eigenvalues, eigenvectors, whirl orbit characteristics, and fluid bearing eccentricities [8].

- **Calculate Steady State Synchronous Response**
  This function calculates the steady-state response of the system to unbalance or a bent rotor, also known as synchronous excitation. It provides the response at all nodes for a vector of rotor spin speeds, facilitating the analysis of operating response for specified spin speeds [8].

- **Calculate the Frequency Response Function**
  For systems where the excitation frequency differs from the rotational speed, the software calculates the frequency response function. It considers multiple degrees of freedom and applies the force simultaneously across these, with the option to specify the direction of rotation for spinners. This feature supports steady-state excitation through foundations and auxiliary bearings [8].

- **Calculate Critical Speeds**
  The software can calculate critical speeds using both direct and iterative methods, depending on the bearing properties. It outputs the critical speeds and corresponding mode shapes, providing an essential tool for identifying and analyzing critical operational speeds [8].

- **Calculate Time Response to Pulse at Foundation**
  The software calculates the time response to a pulse excitation at the foundations. This includes the response at all degrees of freedom, the base excitation displacement, and the time vector. The model can be reduced using Guyan reduction for efficiency [8].

- **Calculate Rundown and Runup**
  This function calculates the response when running through critical speeds, considering a constant acceleration. It outputs the response at all degrees of freedom and the rotor spin speed as a function of time, supporting both rundown and runup simulations [8].

- **Calculate Whirl Orbit Properties**
  After computing the response or mode shapes, the software calculates the properties of whirl orbits, including the direction and dimensions of the response ellipse. This feature is crucial for understanding the dynamic behavior of the rotor system under various operating conditions [8].

These analysis functions in the Cambridge Rotorsol Suite provide comprehensive tools for rotor dynamics analysis, enabling detailed examination of system responses and characteristics under various conditions. The structured approach ensures accurate and reliable results, aiding in the design and optimization of rotor systems.

4.4 Sample Analyses

4.4.1 Timoshenko Beam Element Model - Analysis w/ Gyroscopic Effects

The analysis includes the calculation of mode shapes and natural frequencies, plotting of Campbell diagrams and root loci, visualization of mode shapes, and plotting of whirl orbits. Below is a detailed discussion of how the software performed the analysis, highlighting the input parameters and their locations in the code. The entire configuration file may be seen in Appendix A.

The material properties and model parameters are defined at the beginning of the script. These parameters include Young's Modulus, Shear Modulus, density, and damping factor.

```
E = 211e9;
G = 81.2e9;
rho = 7810;
damping_factor = 0;
model.node = [1 0.0; 2 0.25; 3 0.5; 4 0.75; 5 1.0; 6 1.25; 7 1.50];
```

The disks are defined by their positions, densities, thicknesses, and diameters. The inside diameter of the disks is assumed to be the same as the outer diameter of the shaft.

```
disk1_od = 0.28;
disk2_od = 0.35;
disk_thick = 0.07;
model.disc = [1 3 rho disk_thick disk1_od shaft_od; ...
              1 5 rho disk_thick disk2_od shaft_od];
```

The nodes and shaft elements are also defined here. This is a model with six equal-length Timoshenko beam elements. A graphical representation of the rotor along with disk positions may be seen in Figure 10.

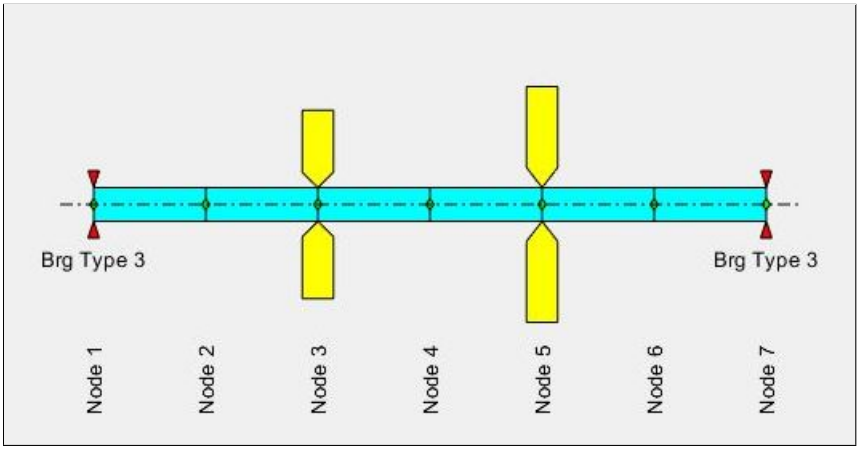

Figure 10: Graphical Representation of the 6-element Shaft

The shaft is modeled using Timoshenko beam elements with gyroscopic effects. The shaft parameters, including type, nodes, outer diameter, inner diameter, density, Young's Modulus, Shear Modulus, and damping factor, are specified in the following section:

```
shaft_od = 0.05;
shaft_id = 0.0;
model.shaft = [2 1 2 shaft_od shaft_id rho E G damping_factor; ...
               2 6 7 shaft_od shaft_id rho E G damping_factor];
```

The bearings are modeled as constant stiffness short isotropic bearings with no damping. The stiffness values are specified for bearings at nodes 1 and 7.

```
bear_stiff = 1e6;
model.bearing = [3 1 bear_stiff bear_stiff 0 0; ...
                 ...
                 3 7 bear_stiff bear_stiff 0 0];
```

The rotor speed is defined as a vector of speeds for plotting the Campbell diagram and root loci (top left and top right graphs in Figure 11 respectively). The analysis functions are called to compute eigenvalues, eigenvectors, and plot the results. Additionally, the rotor speed for mode shape (bottom left of Figure 11) and orbit plotting (bottom right of Figure 11) are also specified.

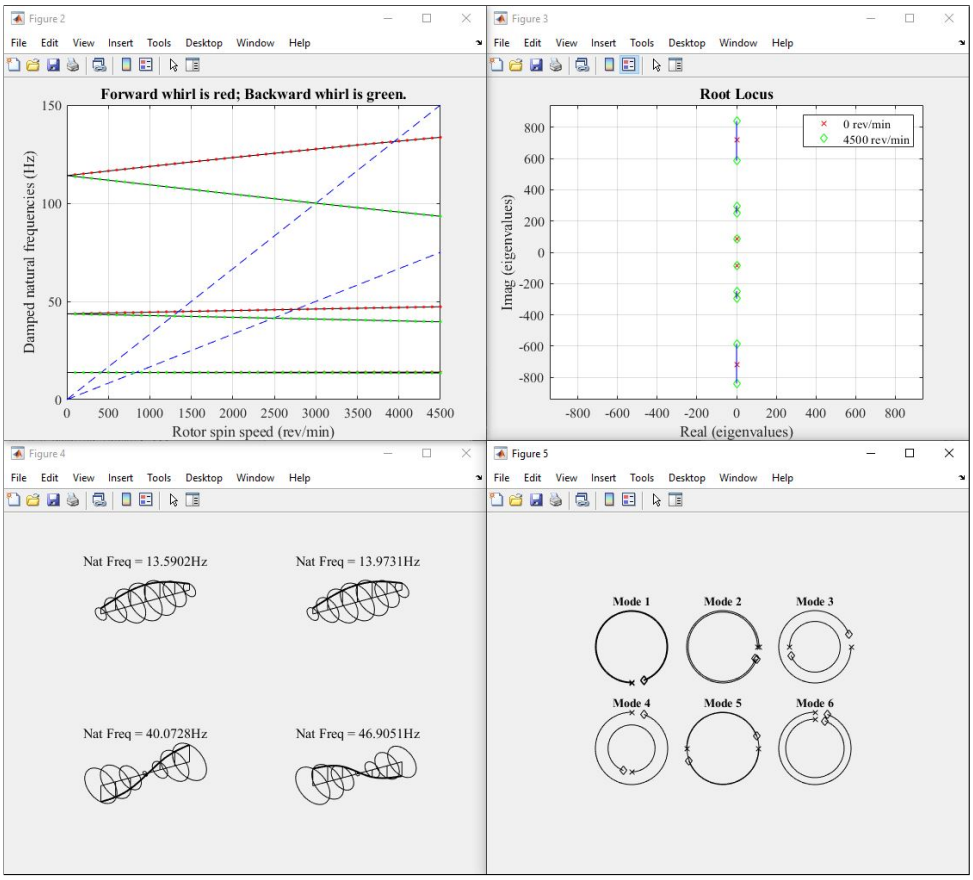

Figure 11: Graphical Representation of Rotordynamics Analysis Results

4.4.2 Mapping Critical Speeds & Associated Mode Shapes

This software suite can be extended in functionality to map critical speeds and associated mode shapes of a rotor dynamic system. For the example analysis presented below the same 6-element shaft, as seen in Figure 10, was analyzed.

The main analysis involves calculating the critical speeds of the rotor using an iterative method for a range of bearing stiffness values, focusing on forward whirling modes. The mode shapes are then normalized and shape functions are used to obtain smooth mode shapes for detailed visualization. The software then generates plots to illustrate the variation of critical speeds and mode shapes with respect to the bearing stiffness, providing insights into the dynamic behavior of the rotor under different conditions. These visualizations help in understanding the rotor's performance and stability, aiding in the design and optimization of the rotor system.

The number of bearing stiffness values to consider is set to 60, and these values are defined using a logarithmic space ranging from 10^5 to $10^{7.3}$. The number of nodes in the model is determined from the size of the node array, and the number of degrees of freedom is calculated as four times the number of nodes. The axial positions of the nodes are extracted, and the number of points within each shaft element is set to 20. The variable `xi` represents normalized positions within an element, ranging from 0 to 1. Shape functions $N1$, $N2$, $N3$, and $N4$ are defined to describe the deformation within each element, providing a smooth interpolation of the mode shapes along the shaft length. The parameters may be entered into the script are as follows:

```
Nk = 60;  % number of bearing stiffness values to consider
RH_bearing_k = logspace(5,7.3,Nk);  % define bearing stiffness values
nnode = size(model.node,1);
ndof = 4*nnode;

z = model.node(:,2);  % axial node positions
n_xi = 20;  % number of points within an element
xi = (0:n_xi).'/n_xi; % points within element
N1 = ones(n_xi+1,1) - 3*xi.^2 + 2*xi.^3;  % shape functions
N2 = xi - 2*xi.^2 + xi.^3;
N3 = 3*xi.^2 - 2*xi.^3;
N4 = -xi.^2 + xi.^3;
```

Parameters for critical speed calculations can be entered as follows:

```
NX = 1;
damped_NF = 1;
number_criticals = 6;
max_iterations = 20;
convergence_tol = 1e-6;
```

One can initialize arrays to store the critical frequencies in RPM and the corresponding mode shapes. It iterates over the range of bearing stiffness values, updating the right-hand side bearing stiffness for each iteration. The model's bearings are redefined with the updated stiffness values, and the critical speeds and mode shapes are calculated using the function `crit_spd`. The critical speeds are converted from radians per second to revolutions per minute and stored in the `critical_freq_map_rpm` array. For each critical speed, the mode shapes are normalized and smoothed using shape functions to produce a detailed representation of the deformation along the shaft. The smoothed mode shapes are stored in the `critical_mode_map` array, allowing for detailed analysis of the mode shapes as a function of bearing stiffness.

```
critical_freq_map_rpm = zeros(number_criticals,Nk);
critical_mode_map = zeros((nnode-1)*(n_xi+1),number_criticals,Nk);

for i=1:Nk

    % set the bearing stiffness
    Bearing_RHcase = RH_bearing_k(i)*[1 1  0   0];
    model.bearing = [3 1 Bearing_LHcase; ...
                     3 5 Bearing_RHcase];
    [critical_speeds,mode_shapes] = crit_spd(model,NX,damped_NF,
    number_criticals,max_iterations,convergence_tol);
    critical_freq_map_rpm(:,i) = critical_speeds(1:number_criticals)*60/(2*pi
    );
    for ic=1:number_criticals
        [mx,index] = max(abs(mode_shapes(1:4:28,ic)));
        mode_ic = mode_shapes(:,ic)/mode_shapes(4*index-3,ic);
        mode_xi = [];
        for inode = 1:nnode-1
            Le = z(inode+1) - z(inode);
            xx = [N1 Le*N2 N3 Le*N4]*real(mode_ic([4*inode-3 4*inode 4*inode
    +1 4*inode+4]));
            mode_xi = [mode_xi; xx];
        end
        critical_mode_map(:,ic,i) = mode_xi;
    end
end
```

One can then use the program to plot the variation of critical speeds with the bearing stiffness, providing a visual representation of how the rotor's critical speeds change with different bearing stiffness values.

The output of the critical speed analysis for different bearing stiffness values can be seen in Figure 12.

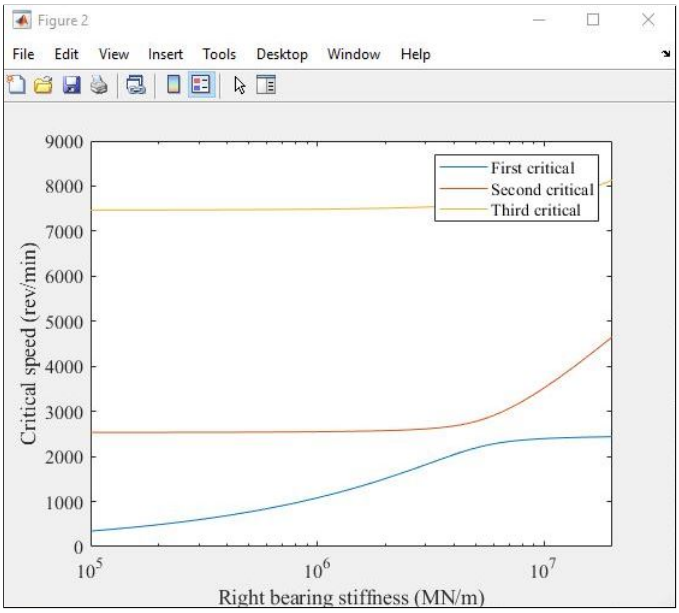

Figure 12: Variation of critical speeds with right bearing stiffness

The mode shapes are also plotted to visualize how they vary with bearing stiffness. This helps in understanding the deformation patterns and dynamic behavior of the rotor under different stiffness conditions. Examples of these plots may be seen in Figures 13, 14, and 15 showing the variation of first, second, and third mode shapes respectively.

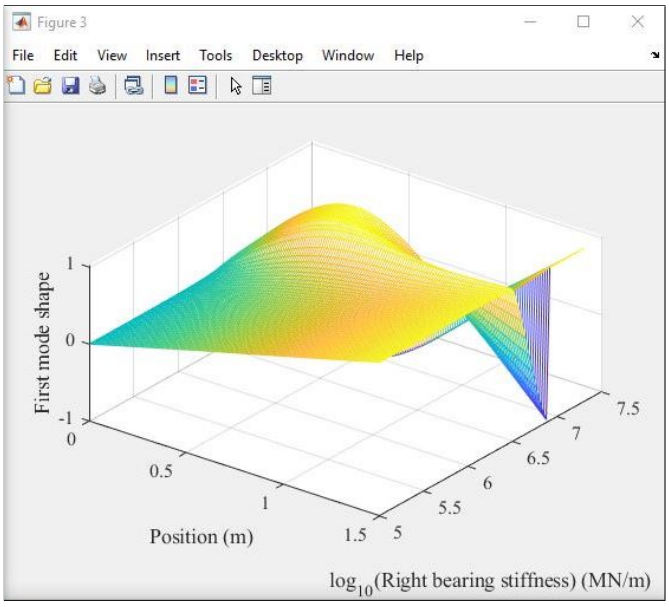

Figure 13: First mode shape variation with right bearing stiffness

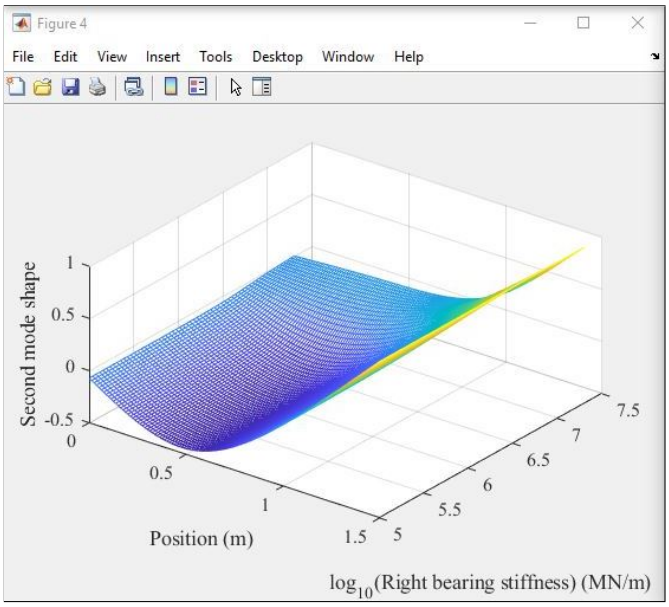

Figure 14: Second mode shape variation with right bearing stiffness

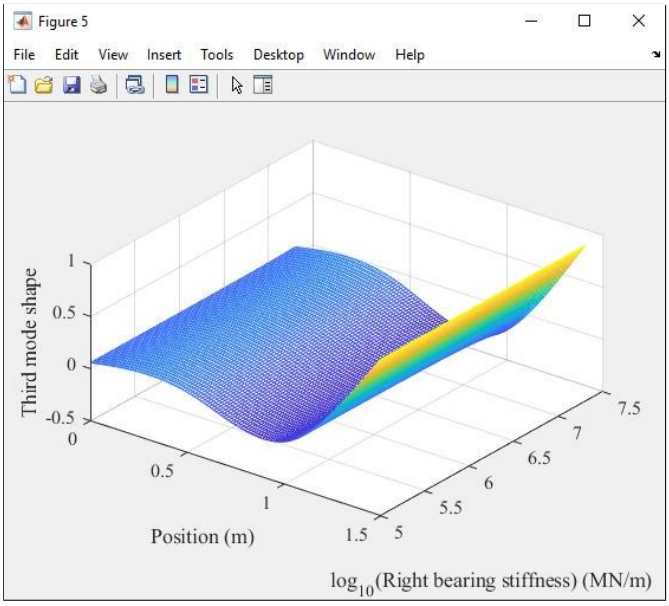

Figure 15: Third mode shape variation with right bearing stiffness

The graph's axes provide essential context for interpreting the rotor's behavior. The x-axis, labeled "Position (m)," represents the axial position along the rotor's length, segmented into specific nodes. The y-axis, labeled "$\log_{10}$(Right Bearing Stiffness) (MN/m)," uses a logarithmic scale to show the bearing stiffness in Mega Newtons per meter, effectively compacting a wide range of stiffness values. The z-axis, labeled "First Mode Shape," depicts the rotor's shape corresponding to its first natural frequency, crucial for understanding its dynamic behavior and stability.

For example, in the graph of the first mode shape variation (Figure 13) Several observations can be made from the surface characteristics. The mode shape varies significantly along the rotor's length, with higher amplitude oscillations in some sections indicating regions more prone to vibrational modes. The mid-sections display smoother mode shapes, while the ends exhibit more pronounced dynamic activity. The bearing stiffness also significantly impacts the mode shape, particularly in the range of 10^6 to 10^7 MN/m. The logarithmic scale reveals that mode shape sensitivity increases with stiffness, with more abrupt changes occurring beyond a stiffness threshold of around 10.5^6 MN/m. This suggests a transition in the rotor system's dynamic behavior, potentially reaching a region where natural frequencies are significantly altered.

This extended analysis in the MATLAB script allows for a deeper understanding of the rotor dynamics by exploring the impact of varying bearing stiffness on critical speeds and mode shapes. Engineers can use this information to minimize vibrational issues by strategically placing additional supports or damping mechanisms in critical regions. The sharp variations at higher stiffness values highlight the necessity for precise control over bearing properties to maintain rotor stability–perhaps accomplished through implementing an AMB.

5 Conclusion

This report highlights the potential for significant advances in rotor dynamics analysis facilitated through the use of a comprehensive software suite. The output of such software can provide valuable insights into the relationship between rotor position, bearing stiffness, and mode shapes, essential for optimizing the design and performance of rotor systems. The findings highlight the importance of fine-tuning bearing stiffness and understanding critical speed variations to enhance rotor stability and avoid resonant conditions.

Future endeavors should focus on the verification and validation of model predictions to ensure accuracy and reliability, especially in the context of TGs where operational integrity is paramount. Validating these models against empirical data will improve confidence in their predictive capabilities and ensure they meet the demands of high-stakes environments.

The examples provided by the software suite demonstrate the fundamental features necessary for conducting robust rotodynamics analyses. These capabilities can be further developed to support more intricate and comprehensive analyses, allowing for advanced rotor dynamics studies. By enabling basic tests to be run before physical iterations, the software significantly reduces the cost and time associated with innovation. This preemptive testing capability ensures that physical prototypes are optimized and potential issues are addressed early in the design process.

The integration of this rotor dynamics analysis software within engineering workflows may enhance the efficiency, reliability, and performance of TGs. By leveraging these tools, engineers can achieve more accurate modeling, better predict dynamic behaviors, and implement effective control strategies to maintain system stability and operational excellence.

6 References

[1] Yoon, S. Y., Lin, Z., Allaire, P. E. (Year). Control of Surge in Centrifugal Compressors by Active Magnetic Bearings: Theory and Implementation. Springer.

[2] Foppl, A., "Das Problem der Lavalschen Turbinenwelle", Der Civilingenieur, Vol 4, pp 335-342, 1895.

[3] Jeffcott, H., "The Lateral Vibration of Loaded Shafts in the Neighborhood of a Whirling Speed-The Effect of Want of Balance", Phil. Mag., Vol 37, No 6, pp 301-314,1919.

[4] Nelson, H. D., "A Finite Rotating Shaft Element Using Timoshenko Beam Theory", ASME Journal of Mechanical Design, Vol. 102, pp 793- 803, 1980.

[5] Genta, Giancarlo, Dynamics of Rotating Systems, Springer, NY, 2005.

[6] Lalanne, Michael and Ferraris, Guy, Rotordynamics Prediction in Engineering, 2nd Edition, John Wiley Sons Ltd., NY, 1998.

[7] Allaire, P.E.: Basics of the Finite Element Method: Solid Mechanics, Heat Transfer, and Fluid Mechanics. Brown, Dubuque (1985)

[8] Friswell, M. I., Penny, J. E. T., Garvey, S. D., Lees, A. W. (2010). Dynamics of Rotating Machines. Cambridge University Press.

A Cambridge Rotorsol Software Suite

Rotor bearing system configuration file with example parameters:

```
clear
format short e
close all
set(0,'defaultaxesfontsize',12)
set(0,'defaultaxesfontname','Times New Roman')
set(0,'defaulttextfontsize',12)
set(0,'defaulttextfontname','Times New Roman')

% set the material parameters
E = 211e9;
G = 81.2e9;
rho = 7810;
damping_factor = 0;   % no damping in shaft

% Consider the model with 6 equal length elements
% Shaft is 1.5m long
model.node = [1 0.0; 2 0.25; 3 0.5; 4 0.75; 5 1.0; 6 1.25; 7 1.50];
% Assume shaft type 2 - Timoshenko with gyroscopic effects included
% Solid shaft with 50mm outside diameter
shaft_od = 0.05;
shaft_id = 0.0;
model.shaft = [2 1 2 shaft_od shaft_id rho E G damping_factor; ...
               2 2 3 shaft_od shaft_id rho E G damping_factor; ...
               2 3 4 shaft_od shaft_id rho E G damping_factor; ...
               2 4 5 shaft_od shaft_id rho E G damping_factor; ...
               2 5 6 shaft_od shaft_id rho E G damping_factor; ...
               2 6 7 shaft_od shaft_id rho E G damping_factor];

% Disk 1 at node 3 has diameter of 280mm and thickness of 70mm
% Disk 2 at node 5 has diameter of 350mm and thickness of 70mm
% Note inside diameter of disk is assumed to be the outside diameter of the
% shaft
disk1_od = 0.28;
disk2_od = 0.35;
disk_thick = 0.07;
model.disc = [1 3 rho disk_thick disk1_od shaft_od; ...
              1 5 rho disk_thick disk2_od shaft_od];

% constant stiffness short isotropic bearing (1NM/m) with no damping
% bearings at the ends - nodes 1 and 7
bear_stiff = 1e6;
model.bearing = [3 1 bear_stiff bear_stiff 0 0; ...
                 3 7 bear_stiff bear_stiff 0 0];

% draw the rotor
figure(1), clf
picrotor(model)
```